JOURNAL OF MATERIALS SCIENCE 33 (1998) 2121–2127

Kinetic analysis of the serial reactions of lead magnesium tungstate ceramics using a multiple core-shell model

CHUNG-HSIN LU*, JIUN-TING LEE
Department of Chemical Engineering, National Taiwan University, Taipei, Taiwan

The solid-state reaction kinetics of a sequential reaction system were analysed theoretically and experimentally. For the reactions occurring in series, $A + R \rightarrow B$ and $B + Q \rightarrow C$, a multiple core–shell diffusion-controlled model has been proposed. The relations between the consumption fractions of A and B and the reaction time under isothermal conditions have been quantitatively deduced. The sequential reactions of $PbWO_4 + PbO \rightarrow Pb_2WO_5$ and $Pb_2WO_5 + MgO \rightarrow Pb(Mg_{1/2}W_{1/2})O_3$ in the formation processes of $Pb(Mg_{1/2}W_{1/2})O_3$ were utilized as the model reactions. The unidirectional diffusion of PbO into $PbWO_4$ to form Pb_2WO_5 and that of MgO into Pb_2WO_5 to generate $Pb(Mg_{1/2}W_{1/2})O_3$ were verified by EDS. The derived equations were confirmed to elucidate accurately the kinetics of the serial reactions in the $Pb(Mg_{1/2}W_{1/2})O_3$ system. Based on the reaction model, the activation energy for the diffusion of MgO into $Pb(Mg_{1/2}W_{1/2})O_3$ was estimated to be 161.7 kJ mol^{-1}.

1. Introduction

The reaction kinetics of solid-state particles have received much attention in the past few decades [1–9]. Several physical models have been developed for analysing solid-state reactions based on different assumptions. In general, these models can be divided into three categories: (a) the diffusion-controlled models, (b) the nucleation-controlled models, and (c) the interface-reaction controlled (phase-boundary) models. For ceramics and metals, the diffusion-controlled models are most often utilized to interpret the correlation between the reaction fraction and the reaction time, because the diffusion of solid-state species is relatively slower than other steps. Jander [1] established the first core–shell model, based on a planar diffusion assumption to correlate the reaction fraction with the reaction time elapsed. The core–shell model based on a three-dimensional diffusion assumption was introduced by Ginstling and Brounshtein [2]. Carter [3] later corrected this model by introducing the consideration of the difference in molar volume between the reactants and products. Although these models can fairly accurately estimate the reaction fraction for powder reactions under certain assumptions, they can only analyse the single reaction system. In other words, the kinetic models for the multiple-step reactions have not yet been investigated thoroughly.

Electronic ceramics usually consist of a complex structure containing two or more atoms. Owing to the complexity of their structures, the complete formation of these materials often requires several reaction steps. In order to control the reaction conditions for obtaining pure compounds with fine microstructures, the understanding of reaction kinetics is indispensable. However, the conventional reaction models are no longer satisfactory for analysing the kinetics in the multiple solid-state reactions. In response to the concern for solving the above problem, this study was focused on the kinetics of two-step serial reactions in the solid-state. A multiple core–shell diffusion-controlled model was proposed. According to this model, the kinetic equations were derived for exploring the relations between reaction fraction and reaction time under isothermal conditions.

In order to confirm the validity of the derived kinetic equations, the formation processes of lead magnesium tungstate, $Pb(Mg_{1/2}W_{1/2})O_3$, were used as the model reaction system. $Pb(Mg_{1/2}W_{1/2})O_3$ is one of the anti-ferroelectric materials having a complex perovskite structure [10]. The $Pb(Mg_{1/2}W_{1/2})O_3$-based solid solutions exhibit excellent dielectric properties, and they have been used for multilayer capacitor applications [11–14]. According to the previous study [15], in the formation processes of $Pb(Mg_{1/2}W_{1/2})O_3$, lead oxide first reacts with tungsten oxide to form lead tungstate, $PbWO_4$, and subsequently $PbWO_4$ reacts with lead oxide to generate Pb_2WO_5. Finally, Pb_2WO_5 reacts with MgO to yield $Pb(Mg_{1/2}W_{1/2})O_3$.

* Author to whom all correspondence should be addressed.

The derived equations are used to analyse the kinetics in the serial reactions during the formation processes of $Pb(Mg_{1/2}W_{1/2})O_3$.

2. Reaction kinetics

In the system of a sphere, A, thoroughly surrounded by reactants R and Q, the solid-state reactions are assumed to occur in series as follows

$$\begin{array}{ccccc} A & + & R & \rightarrow & B \\ 1-x & & 1-x & & x-y \end{array} \quad (1)$$

$$\begin{array}{ccccc} B & + & Q & \rightarrow & C \\ x-y & & 1-y & & y \end{array} \quad (2)$$

x is defined as the consumption fraction of A in Equation 1, and y is defined as the consumption fraction of B in Equation 2, which is expressed as the moles of B consumed in Equation 2 divided by the moles of original A. For analysing the above system, a multiple core–shell model for the serial reactions is proposed as illustrated in Fig. 1. At the initial reaction stage, R reacts with A to produce the product B, and a shell section of B is formed around the unreacted core of A. Once B is formed, Q subsequently reacts with B to produce another outer shell of C. After C is generated, R has to diffuse through both product layers of B and C to reach the surface of the unreacted A for Reaction 1 to continue progressing. In order to simplify the analysis processes, R and Q are assumed to diffuse unidirectionally into A. In other words, the counterdiffusion of A through the product shells is neglected. Furthermore, only the planar diffusion process is taken into consideration.

In the above serial reactions, multiple diffusion steps are involved. First we consider the flux of Q into the product layer C which has a thickness h_1. According to Fick's first law in the plane diffusion, the flux of Q through C, F_{QC}, is expressed as

$$F_{QC} = D_{QC}(C_{Q0} - C_{Q1})/h_1 \quad (3)$$

where C_{Q0} and C_{Q1} are the concentrations of Q on the outer surface of the shells of C and B, respectively, and

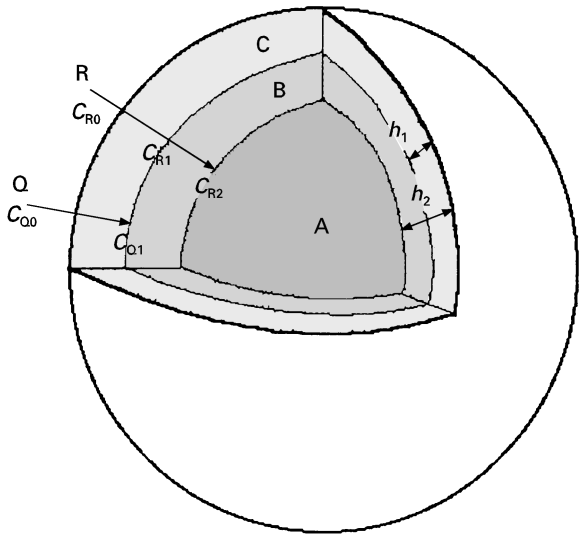

Figure 1 The multiple core–shell model for the serial reactions.

D_{QC} is the diffusion coefficient of Q through the C layer. Considering the mass balance, the flux of Q is proportional to the formation rate of the volume of the C layer. In addition, the formation rate of the volume of C can be assumed to be proportional to that of the thickness of C. Then the following equation can be derived

$$\frac{dh_1}{dt} = m_1 F_{QC} = m_1 D_{QC}(C_{Q0} - C_{Q1})/h_1 \quad (4)$$

where m_1 is a proportional factor. Assume that the reaction mechanism is controlled by the diffusion process, i.e. the reaction rate is faster than the diffusion rate. Therefore, all species of Q reaching the surface of B will quickly react with B and consume part of B, thereby inducing the concentration of C on the outer surface of B to be approximately zero ($C_{Q1} = 0$). On the condition that the bulk concentration of Q (C_{Q0}) is constant and D_{QC} is also constant at the same temperature, from the integration of Equation 4, we obtain

$$h_1 = s_1 t^{1/2} \quad (5a)$$

where

$$s_1 = (2m_1 D_{QC} C_{Q0})^{1/2}. \quad (5b)$$

The flux of the diffusion of R through B and C layers (F_{RC} and F_{RB}) can be expressed as

$$F_{RC} = D_{RC}(C_{R0} - C_{R1})/h_1 \quad (6)$$

and

$$F_{RB} = D_{RB}(C_{R1} - C_{R2})/(h_2 - h_1) \quad (7)$$

where h_2 is the sum of the thickness of B and C layers, D_{RC} and D_{RB} are the diffusion coefficients of R through the C and B layers, and C_{R0}, C_{R1}, and C_{R2} represent the concentrations of R on the outer surface of C, B, and A, respectively. Because Reaction 1 is also diffusion-controlled, C_{R2} can be regarded as zero. Assuming no consumption of R during the diffusion process, we can presume $F_{RC} = F_{RB}$. From Equations 6 and 7, we obtain

$$C_{R1} = D_{RC}C_{R0}/[D_{RB}h_1/(h_2 - h_1) + D_{RC}] \quad (8)$$

Substituting Equation 8 into Equation 7 gives

$$F_{RB} = D_{RB}D_{RC}C_{R0}/[(D_{RB} - D_{RC})h_1 + D_{RB}h_2] \quad (9)$$

Because the thickening rate of product B is also proportional to the flux of R through B, we obtain

$$\frac{dh_2}{dt} = m_2 F_{RB} = m_2 D_{RB}D_{RC}C_{R0}/[(D_{RB} - D_{RC})h_1 + D_{RB}h_2] \quad (10)$$

where m_2 is a constant. Substituting Equation 5 into Equation 10 and integrating Equation 10 results in

$$h_2 = s_2 t^{1/2} \quad (11a)$$

where

$$s_2 = (2m_1 D_{QC} C_{Q0})^{1/2}(1 - D_{RB}D_{RC}) + (2m_1 D_{QC} C_{Q0}(1 - D_{RB}/D_{RC})^2 + 2m_2 D_{RB} C_{R0})^{1/2} \quad (11b)$$

Reaction fractions x and y can be expressed in terms of the volume fraction of the product layers. Therefore, we have

$$x = (V_B + V_C)/V_0 = 1 - [(r_0 - h_2)/r_0]^3 \quad (12)$$

and

$$y = V_C/V_0 = 1 - [(r_0 - h_1)/r_0]^3 \quad (13)$$

where V_0 and r_0 are the original volume and radius of sphere A, V_B and V_C are the volumes of B and C, respectively. Substitution of Equations 5 and 11 into Equations 12 and 13 results in

$$[1 - (1 - x)^{1/3}]^2 = k_1 t \quad (14)$$

$$[1 - (1 - y)^{1/3}]^2 = k_2 t \quad (15)$$

where $k_1 = (s_2)^2/r_0^2$ and $k_2 = (s_1)^2/r_0^2$. Consequently, Equations 14 and 15 can be used to express the relations between conversions and reaction time for serial reactions under isothermal conditions. These equations exhibit a similar form to that of Jander's equation [1].

3. Experimental procedure

Proportionate amounts of reagent-grade starting materials PbO, MgO, and WO_3 were mixed together according to the composition of $Pb(Mg_{1/2}W_{1/2})O_3$ and were ball-milled for 48 h with ethyl alcohol using zirconia balls in a polyethylene jar. Following drying in a rotary evaporator under reduced pressure, the dried powder was used as the starting materials of $Pb(Mg_{1/2}W_{1/2})O_3$.

In order to understand the reaction kinetics, the mixed powder was uniaxially pressed into pellets under 196 MPa and heated under isothermal conditions. The pellets were rapidly put into a pre-heated furnace set at the desired temperature (from 500–600 °C) for a certain period of heating time. Then the pellets were pulled out from the hot zone and quenched in air. The compounds present in the heated specimens were identified via X-ray powder diffraction (XRD) analysis using CuK_α radiation. The actual content of each phase present in the specimens was determined by the internal standard method. For obtaining the calibration lines, different ratios of silicon powder and each single species were mixed and analysed using X-ray diffraction. The ratio of the intensity of the major diffraction peak of silicon to that of the single phase, I_i/I_{Si}, was plotted against the weight ratio, W_i/W_{Si}. Then the proportional factors of the intensity ratio to the weight ratio were applied to calculate the conversion of the serial reactions. Microstructure and chemical composition of specimens were studied via a scanning electron microscrope (SEM) coupled with energy dispersive X-ray spectroscopy (EDS).

4. Results and discussion

4.1. Isothermal reactions of $Pb(Mg_{1/2}W_{1/2})O_3$

The starting materials of $Pb(Mg_{1/2}W_{1/2})O_3$ were isothermally heated at temperatures ranging from 500–600 °C for various heating times. The representative XRD patterns of the specimens heated at 500 and 600 °C are illustrated in Fig. 2a and b, respectively. In addition, the relative contents of each phase present in specimens versus reaction time are summarized in Fig. 3 to indicate the formation diagrams at various temperatures. The relative content of each phase was calculated from the ratio of the intensity of the major diffraction peak of each phase to the sum of the intensity of the major peak of all phases present in specimens. Fig. 2a indicates that, after the specimens were heated at 500 °C for a short period, a large amount of $PbWO_4$ and a small amount of Pb_2WO_5 and $Pb(Mg_{1/2}W_{1/2})O_3$ were formed; however, no WO_3 was found. In the mixtures of the starting materials of $Pb(Mg_{1/2}W_{1/2})O_3$, WO_3 is the limiting species; hence, once WO_3 is entirely consumed, the formation of $PbWO_4$ can be considered to be complete. Therefore, in the following analysis, only the reactions for the formation of Pb_2WO_5 and $Pb(Mg_{1/2}W_{1/2})O_3$ need to be analysed.

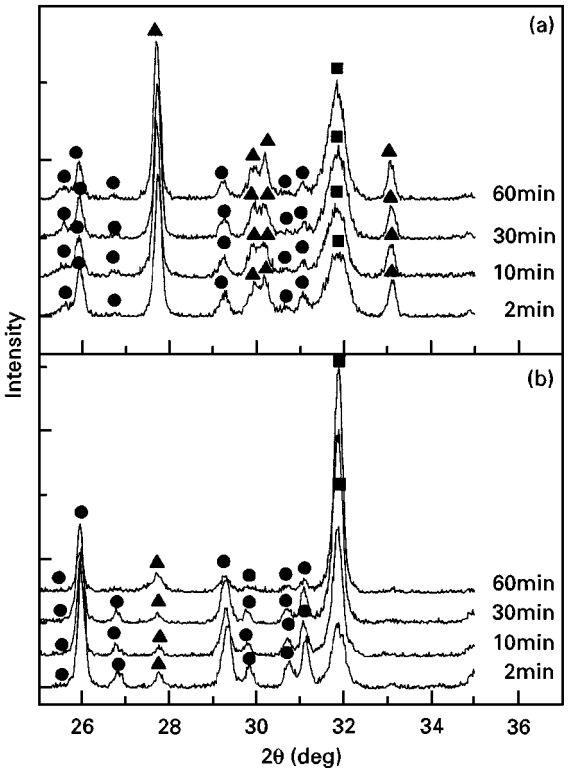

Figure 2 X-ray diffraction patterns of the starting materials of $Pb(Mg_{1/2}W_{1/2})O_3$ heated at (a) 500 °C and (b) 600 °C for various reaction times. (■) $Pb(Mg_{1/2}W_{1/2})O_3$, (▲) $PbWO_4$, (●) Pb_2WO_5.

Fig. 3a shows that during the isothermal reaction at 500 °C, the amount of $PbWO_4$ decreased and that of $Pb(Mg_{1/2}W_{1/2})O_3$ increased with the increasing reaction time. The amount of Pb_2WO_5 increased at first in a short reaction period and then reduced. This phenomenon implies that the Pb_2WO_5 formed in the initial stage of the reactions was consumed later, and the formation process of Pb_2WO_5 will complete with its consumption process. At 550 and 575 °C, the formation diagrams (see Fig. 3b and c) were similar to that at 500 °C. During the 600 °C reaction, the amount of Pb_2WO_5 monotonically reduced with reaction

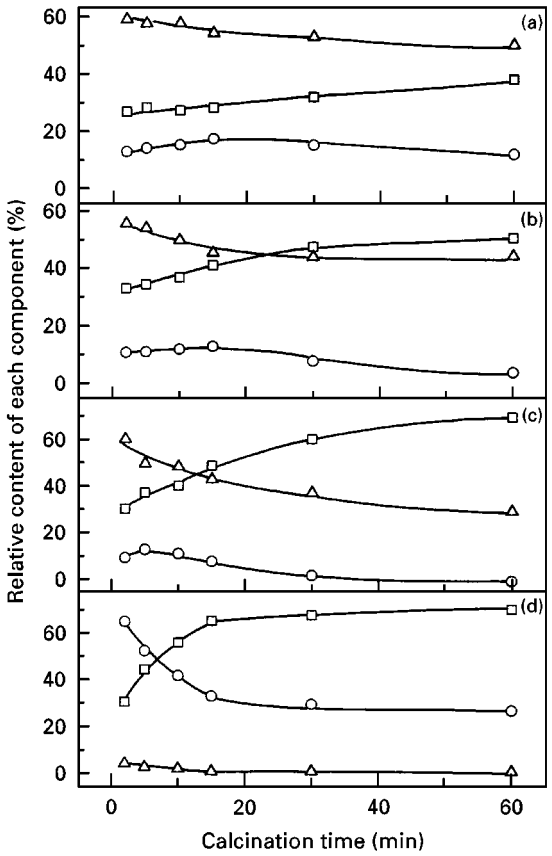

Figure 3 Relative contents of products formed in the isothermal reactions for the starting materials of $Pb(Mg_{1/2}W_{1/2})O_3$ heated at (a) 500 °C, (b) 550 °C, (c) 575 °C, and (d) 600 °C. (△) $PbWO_4$, (○) Pb_2WO_5, (□) $Pb(Mg_{1/2}W_{1/2})O_3$.

time. In addition, the amount of Pb_2WO_5 at the initial stage at 600 °C was significantly higher than that at the other three temperatures. In the examined temperature range, when the reaction temperature rose, the final content of $Pb(Mg_{1/2}W_{1/2})O_3$ after 60 min substantially increased. When the temperature was elevated from 500 °C to 600 °C, the $Pb(Mg_{1/2}W_{1/2})O_3$ yield increased from 40% to 70%. On the contrary, the amount of residual $PbWO_4$ after 60 min was greatly reduced with the reaction temperature.

In order to ensure whether or not the reaction system of $Pb(Mg_{1/2}W_{1/2})O_3$ is unidirectional-diffusion, the experiments of the diffusion couples for $PbWO_4$–PbO and Pb_2WO_5–MgO were carried out. Pure $PbWO_4$ was pressed with PbO under 196 MPa to form pellets, and so were pure Pb_2WO_5 and MgO. These pellets were heated at 600 °C for 2 h and analysed by SEM and EDS. The microstructures of the boundary of the heated pellets are shown in Fig. 4a and b. After 600 °C heating, on the PbO side in the $PbWO_4$–PbO couples, only a trace of tungsten was detected. However, on the other side, the atomic ratio of Pb : W was approximately 2 : 1, implying that Pb_2WO_5 was formed (as shown in Fig. 4a). This confirms that the lead species unidirectionally diffuses into the $PbWO_4$ to form Pb_2WO_5, and the counter-diffusion of tungsten into the PbO can be neglected. In the Pb_2WO_5–MgO couples, only a small amount of lead and tungsten was detected on the MgO side, whereas on the boundary of the Pb_2WO_5 side, EDS

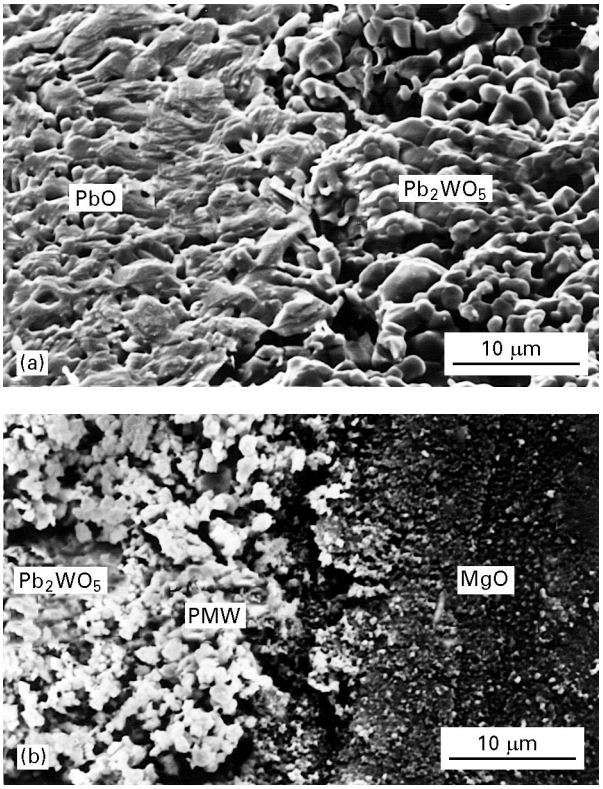

Figure 4 Scanning electron micrographs of the diffusion couples of (a) PbO–$PbWO_4$ and (b) MgO–Pb_2WO_5 heated at 600 °C. PMW $Pb(Mg_{1/2}W_{1/2})O_3$.

results indicated that $Pb(Mg_{1/2}W_{1/2})O_3$ was formed. These results imply that MgO unidirectionally diffuses into the Pb_2WO_5 layer to form $Pb(Mg_{1/2}W_{1/2})O_3$, and the opposite diffusion of lead and tungsten species into the MgO layer can be disregarded.

4.2. Reaction kinetics of $Pb(Mg_{1/2}W_{1/2})O_3$

In order to analyse the reaction kinetics, the conversion of each reaction first has to be calculated. The formation of $Pb(Mg_{1/2}W_{1/2})O_3$ can be described through the following two reactions

$$\underset{1-x}{PbWO_4} + \underset{1-x}{PbO} \rightarrow \underset{x-y}{Pb_2WO_5} \quad (16)$$

$$\underset{x-y}{Pb_2WO_5} + \underset{1-y}{MgO} \rightarrow \underset{2y}{2Pb(Mg_{1/2}W_{1/2})O_3} \quad (17)$$

Using the similar definition of x and y in Equations 1 and 2, x is defined to be the consumption fraction of $PbWO_4$ in Equation 16, and y as that of Pb_2WO_5 in Equation 17. We also define u_1 and u_2 as the molar ratios of $Pb(Mg_{1/2}W_{1/2})O_3$ to Pb_2WO_5, and Pb_2WO_5 to $PbWO_4$, respectively. Then u_1 and u_2 can be expressed as

$$u_1 = N_{Pb(Mg_{1/2}W_{1/2})O_3}/N_{Pb_2WO_5} = (W_{Pb(Mg_{1/2}W_{1/2})O_3}/M_{Pb(Mg_{1/2}W_{1/2})O_3})/(W_{Pb_2WO_5}/M_{Pb_2WO_5}) \quad (18)$$

and

$$u_2 = N_{Pb_2WO_5}/N_{PbWO_4} = (W_{Pb_2WO_5}/M_{Pb_2WO_5})/(W_{PbWO_4}/M_{PbWO_4}) \quad (19)$$

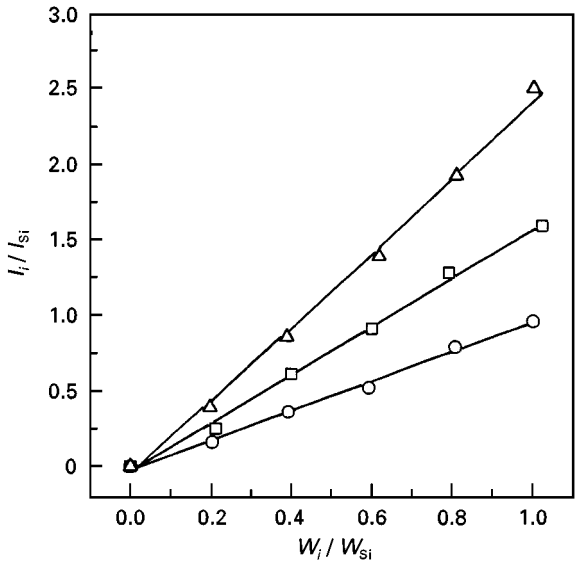

Figure 5 The intensity ratio of each phase to silicon versus the weight ratio of that phase to silicon. (□) $Pb(Mg_{1/2}W_{1/2})O_3$, (○) Pb_2WO_5, (△) $PbWO_4$.

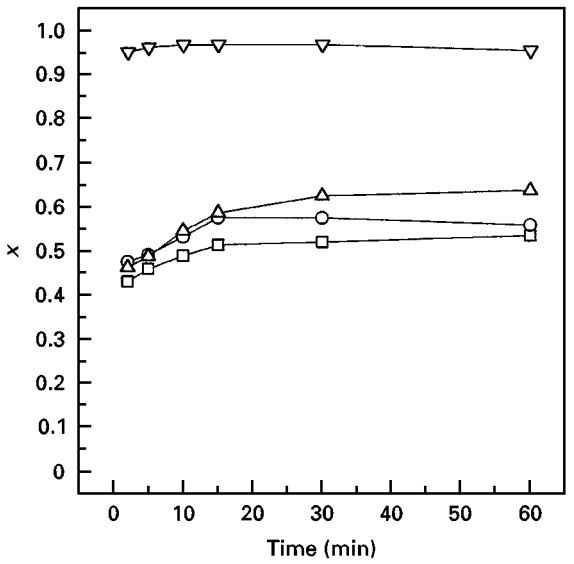

Figure 6 Variation of the conversion x versus reaction time at various temperatures (□) 500 °C, (○) 550 °C, (△) 575 °C, (▽) 600 °C.

where N_i, W_i and M_i are the mole number, weight, and molecular weight of the species i. Using the internal standard method, the relation between the diffraction intensity ratio of each phase to silicon and the weight ratio of that phase to silicon was obtained. As illustrated in Fig. 5, the proportional factors of the diffraction intensity ratio to the weight ratio for $PbWO_4$, Pb_2WO_5, and $Pb(Mg_{1/2}W_{1/2})O_3$ were determined, respectively, as

$$I_{PbWO_4}/I_{Si} = 2.51 W_{PbWO_4}/W_{Si} \quad (20)$$

$$I_{Pb_2WO_5}/I_{Si} = 0.99 W_{Pb_2WO_5}/W_{Si} \quad (21)$$

$$I_{Pb(Mg_{1/2}W_{1/2})O_3}/I_{Si} = 1.63 W_{Pb(Mg_{1/2}W_{1/2})O_3}/W_{Si} \quad (22)$$

Substitution of Equations 20, 21, and 22 into Equations 18 and 19 gives

$$u_1 = 1.15 I_{Pb(Mg_{1/2}W_{1/2})O_3}/I_{Pb_2WO_5} \quad (23)$$

$$u_2 = 1.70 I_{Pb_2WO_5}/I_{PbWO_4} \quad (24)$$

From the definition of x and y in Equations 16 and 17, we can write that $u_1 = 2y/(x - y)$, and $u_2 = (x - y)/(1 - x)$. Therefore, x and y can be expressed in terms of u_1 and u_2 as below

$$x = (2u_2 + u_1u_2)/(2 + 2u_2 + u_1u_2) \quad (25)$$

$$y = u_1u_2/(2 + 2u_2 + u_1u_2) \quad (26)$$

According to the results in Fig. 3, the values of u_1 and u_2 at each reaction time and temperature were calculated using Equations 23 and 24 at first, and then u_1 and u_2 were substituted into Equations 25 and 26 to obtain x and y. Figs 6 and 7 illustrate the relation of the conversions x and y with time at different temperatures, respectively. Both x and y increased with an increase in reaction time and reaction temperature. Once the temperature reached 600 °C, the conversion x approached an equilibrium value of 0.97 after a short period of reaction time. This implies that the transformation of Pb_2WO_5 from $PbWO_4$ was nearly

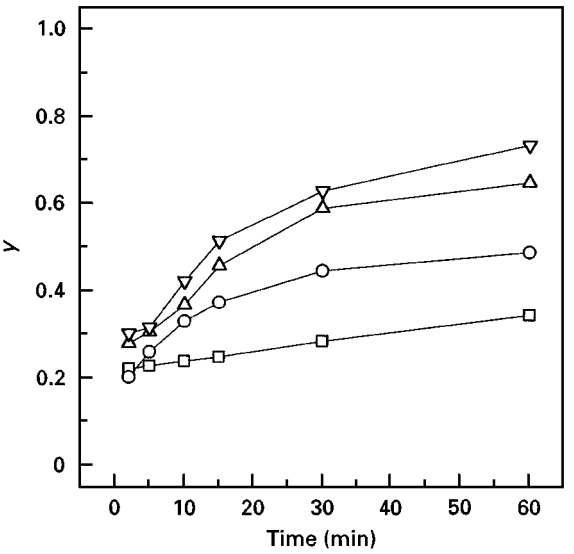

Figure 7 Variation of the conversion y versus reaction time at various temperatures: (□) 500 °C, (○) 550 °C, (△) 575 °C, (▽) 600 °C.

complete. After reaction at 600 °C for 60 min, the value of y approached 0.72.

Because the conversion x at 600 °C reached an equilibrium value after a short reaction period, these equilibrium states were not suitable for kinetic analysis. Therefore, we only substituted the conversion x at 500, 550, and 575 °C into Equation 14. The obtained results are illustrated in Fig. 8. As shown in this figure, the function of $[1 - (1 - x)^{1/3}]^2$ indicated a good linearity with reaction time at all temperatures, revealing the validity of Equation 14 for the reaction kinetics in $Pb(Mg_{1/2}W_{1/2})O_3$. The slopes of the lines in Fig. 8 increased as the reaction temperature rose. However, based on Equation 14, the value of the slope contains a complex function of diffusion coefficients and concentrations; therefore these slopes could not be used as a basis for calculating the activation energy of the reaction.

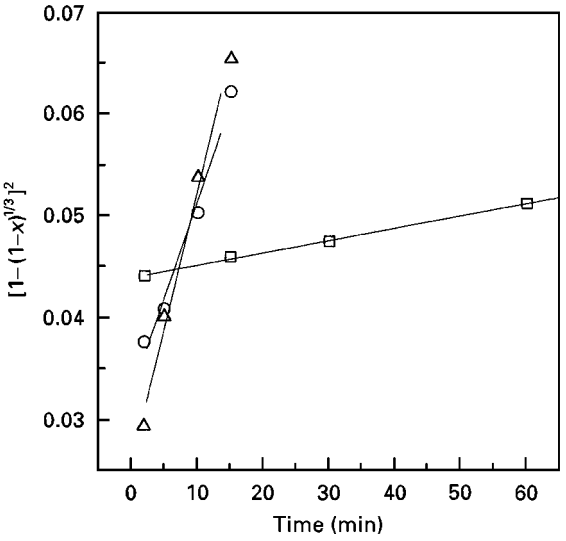

Figure 8 Plot of the function $[1-(1-x)^{1/3}]^2$ versus reaction time at various temperatures: (□) 500 °C, (○) 550 °C, (△) 575 °C.

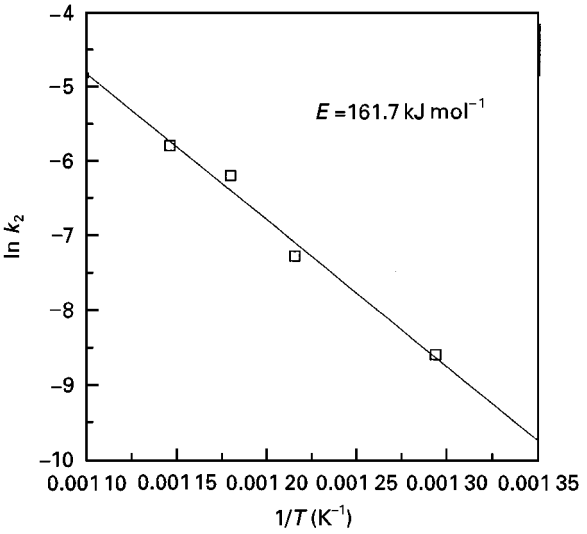

Figure 10 Plot of ln k_2 versus $1/T$ for the reaction kinetics of $Pb(Mg_{1/2}W_{1/2})O_3$.

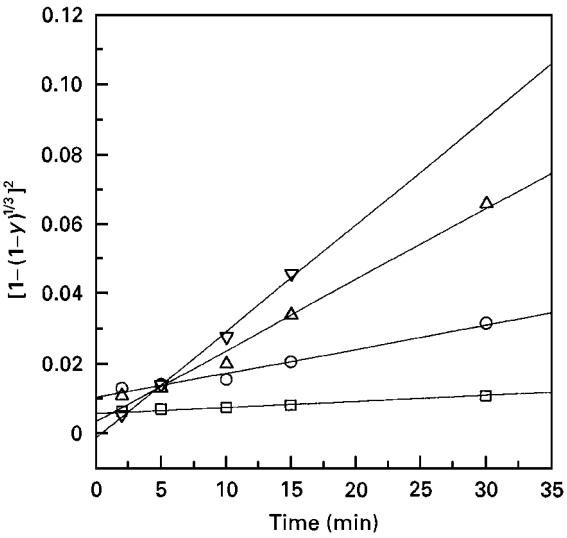

Figure 9 Plot of the function $[1-(1-y)^{1/3}]^2$ versus reaction time at various temperatures: (□) 500 °C, (○) 550 °C, (△) 575 °C, (▽) 600 °C.

Fig. 9 shows the function of $[1-(1-y)^{1/3}]^2$ plotted against reaction time for the reaction temperatures ranging from 500–600 °C. This figure reveals that there is a remarkable linear dependence of $[1-(1-y)^{1/3}]^2$ on reaction time. According to Equation 15, the slopes of the straight lines in Fig. 9 are k_2. Because $k_2 = s_1^2/r_0^2$ and $s_1 = (2m_1D_{QC}C_{Q0})^{1/2}$ (from Equation 5), $k_2 = (2m_1D_{QC}C_{Q0})r_0^2$. The general expression for diffusion coefficient can be expressed as

$$D = D_0 \exp(-E/R/T) \tag{27}$$

where D_0 is a temperature-independent constant, E the activation energy for diffusion, R the gas constant, T the absolute temperature. Because the other terms except D_{QC} in k_2 are temperature-independent, the slope in the plot of $\ln(k_2)$ against the reciprocal of the absolute temperature can obtain the activation energy of diffusion. Fig. 10 illustrates the plot of $\ln(k_2)$ versus $1/T$. This figure shows that a straight line was obtained. From the slope of this line, the activation energy was calculated to be 161.7 kJ mol^{-1}. This value indicates the energy barrier for MgO to diffuse into the $Pb(Mg_{1/2}W_{1/2})O_3$ layer. Consequently, the above results of Figs 8 and 9 confirm that the kinetic equations derived in Section 2 can sufficiently analyse the reaction kinetics for the serial reactions in the formation of $Pb(Mg_{1/2}W_{1/2})O_3$.

It is noted that in the initial reaction the amount of Pb_2WO_5 was low at temperatures lower than 600 °C; however, its amount increased at 600 °C. From Equations 16 and 17 it can be found that the formation of Pb_2WO_5 from $PbWO_4$ competes with the consumption of Pb_2WO_5 for forming $Pb(Mg_{1/2}W_{1/2})O_3$. Below 600 °C, the reaction rate for the formation of Pb_2WO_5 (Equation 16) was lower than that for the consumption of Pb_2WO_5 (Equation 17). Therefore, as long as Pb_2WO_5 is formed, the rapid formation of $Pb(Mg_{1/2}W_{1/2})O_3$ will consume Pb_2WO_5 in a short period, which results in the residual amount of Pb_2WO_5 being small. Nevertheless, at 600 °C, the formation rate of Pb_2WO_5 (Equation 16) is greater than that of $Pb(Mg_{1/2}W_{1/2})O_3$ (Equation 17); hence, a large amount of Pb_2WO_5 remains in the specimens. Because the reaction rate of Equation 16 increases more than that of Equation 17 at high temperatures, the temperature effect on Equation 16 is more prominent.

5. Conclusions

For the reactions occurring in series: A + R → B and B + Q → C, a multiple core–shell model was proposed. Based on the definition for the consumption fractions of A and B (x and y, respectively), the correlations between the consumption fractions and the reaction time under isothermal conditions were theoretically deduced to be $[1-(1-x)^{1/3}]^2 = k_1t$ and $[1-(1-y)^{1/3}]^2 = k_2t$. The sequential reactions

of $PbWO_4 + PbO \rightarrow Pb_2WO_5$ and $Pb_2WO_5 + MgO \rightarrow Pb(Mg_{1/2}W_{1/2})O_3$ in the formation processes of $Pb(Mg_{1/2}W_{1/2})O_3$ were utilized to be the model system. From the diffusion-couple experiments, the unidirectional diffusion of PbO into $PbWO_4$ to form Pb_2WO_5 and that of MgO into Pb_2WO_5 to generate $Pb(Mg_{1/2}W_{1/2})O_3$ were verified. Based on the obtained results, the derived functions of x and y displayed a remarkably linear dependence with reaction time, which confirmed the validity of the above kinetic equations. In addition, the activation energy for the diffusion of MgO into Pb_2WO_5 was estimated to be 161.7 kJ mol^{-1}. The proposed model and equations were confirmed to elucidate accurately the kinetics of the serial solid-state reactions.

Acknowledgement

The authors thank the National Science Council, Taiwan, for financial support of this study under Contract no. NSC 83-0404-E002-071.

References

1. W. JANDER, *Z. Anorg. Allg. Chem.* **163** (1927) 1.
2. A. M. GINSTLING and B. I. BROUNSHTEIN, *J. Appl. Chem. USSR* **23** (1950) 1327.
3. R. E. CARTER, *J. Chem. Phys.* **34** (1960) 2010.
4. M. AVRAMI, *ibid.* **7** (1939) 1103.
5. S. SHARP, G. W. BRINDLEY and B. N. NARAHARI ACHAR, *J. Am. Ceram. Soc.* **49** (1966) 379.
6. J. BERETKA, *ibid.* **67** (1984) 615.
7. E. A. GIESS, *ibid.* **46** (1963) 374.
8. J. R. FRADE and M. CABLE, *ibid.* **75** (1992) 1949.
9. J. BERETKA and T. BROWN, *ibid.* **66** (1983) 383.
10. G. A. SMOLENSKII, N. N. KRAINIK and A. I. AGRANOVSKAYA, *Sov. Phys. Solid State* **3** (1961) 714.
11. W. K. CHOO and M. H. LEEJ, *J. Appl. Phys.* **53** (1982) 7355.
12. S. NOMURA, S. J. JANG, L. E. CROSS and R. E. NEWNHAM. *J. Am. Ceram. Soc.* **62** (1979) 485.
13. Y. YAMASHITA, H. KANAI and O. FURUKAWA, *Jpn, J. Appl. Phys.* **32** (1993) 4265.
14. K. TSUZUKU and M. FUJIMOTO, *J. Am. Ceram. Soc.* **77** (1994) 1452.
15. C. H. LU, *J. Mater. Sci.* **31** (1996) 699.

Received 6 December 1996
and accepted 5 December 1997